applied sciences

MDPI

Article

Effect of Vibration on Automotive Transmission Radial Lip Seal Leakage

Petros Nomikos [1,2], Nick Morris [1], Ramin Rahmani [1,*] and Homer Rahnejat [1,3]

[1] Wolfson School of Mechanical, Electrical and Manufacturing Engineering, Loughborough University, Loughborough LE11 3TU, UK
[2] Neapco Europe GmbH, 52351 Dueren, Germany
[3] School of Engineering, University of Lancashire, Preston PR1 1JN, UK
* Correspondence: r.rahmani@lboro.ac.uk

Abstract

The European Union's regulatory mandate requirements for vehicular components include the integrity of sealing performance, mitigating leaks from fuel tanks and transmission systems in order to guard against environmental pollution. Non-compliance can result in significant costs for the OEM and their supplier base. The majority of the reported research regarding leakage from radial lip seals focuses on static analysis of leakage under a given set of laboratory conditions. However, in practice, seal conjunctions are often subjected to significant excitations due to vehicular vibration. In the current study, the case of a front-wheel drive vehicle, equipped with three-axle accelerometers and subjected to a comprehensive road test, is used as the basis for the development of a realistic representative test rig. The test rig is developed using bespoke components from the vehicle under investigation to assess the impact of the encountered natural frequencies on sealing performance in controlled laboratory conditions, when the system is subjected to controlled excitation. Experiments are conducted to evaluate leakage at the transmission interface, focusing specifically on the sealing system's performance. The influence of driveshaft manufacturing processes using corundum grinding and subsequent surface topography upon leakage performance are also considered. Identified modal response frequencies are imposed upon the test rig using a shaker, whilst the seal leakage is measured. The importance of shaft roughness characteristics, such as topographical skewness upon seal leakage rate under various resonant conditions, are ascertained. The results indicate potentially significant leakage rates under excitation conditions, with a non-optimised shaft roughness profile.

Keywords: vibration; automotive drivetrain; lip seals; sealing surface topography; oil leakage

Academic Editor: Ján Dižo

Received: 16 January 2026
Revised: 2 March 2026
Accepted: 4 March 2026
Published: 16 March 2026

1. Introduction

Leakage of lubricant from automotive drivetrain seals is a well-known concern. A sealing system is formed by the lip of a rotary shaft seal (Radialwellendichtring: RWDR) and the sealing seat of the propeller shaft. In 1938, the first functional RWDR was patented by Simmer [1]. The RWDR provides three main functions at the interface between a driveshaft and gearbox housing. Firstly, it is intended to prevent the leakage of oil, thus maintaining the functional performance of the transmission system. Secondly, it should prevent the incursion of environmental contaminants into the transmission housing, which can damage the powertrain. Thirdly, the sealing system must protect the environment from pollution caused by lubricant leakage.

Leakage invariably occurs from the transmission system, especially in older vehicles. This is reflected, for example, by the statistics shown in Figure 1, provided by TÜV [2], illustrating the failure rate of vehicles by age, between 3 and 11 years.

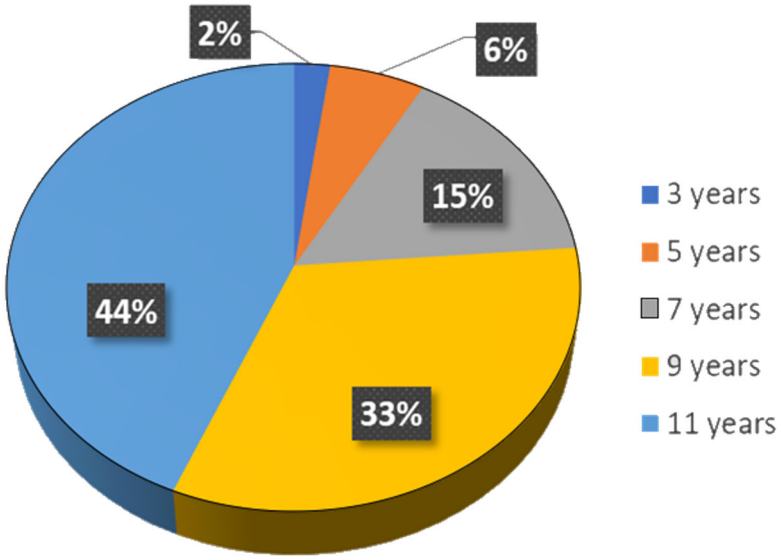

Figure 1. Occurrence of leakage with passenger car age [2].

Significant leakage can occur at even earlier stages in a vehicle's life (e.g., even during the running-in period). Therefore, it is important to investigate the response frequencies that occur in the sealing gap during usual vehicle use and observe their influence on the sealing performance and leakage behaviour. Factors influencing leakage include the shaft lead, lack of coaxial fitment and operating conditions such as shaft speed, contact temperature, seal material, ageing, lubricant rheology and physical chemistry. Additionally, the surface topography of the sealing lip affects the leakage of oil.

In an early contribution, Jagger [3] showed that a continuous film of lubricant is usually formed between the sealing lip and the rotating shaft. He noted the formation of a meniscus at the air/oil boundary, retaining a film of lubricant formed through surface tension. Later, the geometry and material of the RWDR were described in the normative standards, such as DIN 3761-9:1984-01 [4], RMA OS1-1 [5] and DIN ISO 6194-1 [6]. Aside from contact geometry and applied contact load, shaft rotational speed has a significant impact on the sealing behaviour. Salant [7] presented a numerical model to predict the performance of a RWDR under standard operating conditions, where a meniscus is formed on the air side of the seal. He was able to show that the position of the meniscus in the sealing gap is speed-dependent, and above a critical speed, the meniscus is pulled into the sealing zone. Due to the motion of the meniscus towards the oil side, a risk of direct contact between the lip seal and the shaft counter face asperities exists.

Upper [8] developed a model to determine the contact temperature distribution inside a rotary shaft seal. He was able to show that due to the higher thermal conductivity of the shaft, the temperature at the seal surface remains at a higher temperature than that of the shaft surface. Kang and Sadeghi [9] presented a lip seal contact numerical model, based on the simultaneous solution of Reynolds and energy equations to determine the generated heat in the lubricant film. It was shown that the leakage rates increased significantly with elevated temperatures. This was expected, as any temperature rise reduces the viscosity of the lubricant.

A critical factor influencing the sealing performance is the topography of the mating contacting surfaces. Buhl [10] suggested that the active lubricant conveyance effect occurs

along the shaft, as well as at the sealing lip. This effect is as the result of directional surface structures formed during the machining of a shaft, creating a shaft surface lead. Salant [11] presented a numerical model showing that even small changes in the topography of a shaft can induce hydrodynamic effects in the sealing zone, which can significantly affect its performance. Kozuch et al. [12] showed that the skewness of the surface topography correlates well with the lubricant leakage rate. The numerical model verified by surface measurements on the shaft surface confirmed that the lubricant mass flow rate is reduced in the case of negative skewness of the surface topography [12].

There is a dearth of experimental studies based on the representative test rig measurements of the sealing performance of RWDR when affected by lateral and radial vibrations in a real powertrain system. Amabili et al. [13] investigated the dynamic behaviour of RWDR with a test set up, comprising a housing, an RWDR and a disc as a substitute for the driveshaft. The test set up was excited by a shaker (an exciter). Frequency Response Functions (FRFs) were determined for different levels of excitation between the sealing lip and the disc. The results provided an indication of the non-linear vibration behaviour of a sealing system. However, influential factors such as surface topography, temperature and lubrication were neglected. Based on their findings, Silvestri and Prati [14] described the influence of radially induced vibrations on the sealing performance. The aim of their combined experimental and FEA-based numerical analysis was to characterise the effect of different excitation signals on the working temperature of the seal. The sealing lip clearance was dynamically altered and measured using a strain gauge transducer. The results showed that for speeds exceeding 1800 rpm, the sealing lip separated from the shaft surface, causing leakage of the lubricant.

In general, there should be an appropriate prognostic and health monitoring approach for the rotating systems, which would depend on the source of excitation, such as the various methodologies highlighted by Lee et al. [15]. For example, Talikoti et al. [16] provided an overview of the current state of the art in vibration analysis developed for crankshafts of internal combustion engines, which are subjected to a combination of inertial imbalances and the spectral signature of the combustion process itself. Some of the spectral content transmitted onto the transmission input shaft as an output of crankshaft vibrations. For the case of gearbox casing, Kumar and Patil [17] reported vibration analysis predicted by FEA. However, the influence of the resulting vibrations on the sealing performance was not discussed in these contributions. Rather, the noise emissions from the powertrain associated with the vibrations were only considered. Examples of time–frequency representations of gear vibrations, causing damage to gears and bearings of the powertrain system, were provided by Oehlmann et al. [18]. Tuma [19] provided an overview of practical methods for the palliation of vibrations, for sources of undesired noise emissions from gearboxes and transmission units. Lei et al. [20] used an adaptive stochastic resonance method to investigate the weak points of differential casings. The results were verified using a test rig. However, none of these contributions related to the sealing performance, particularly the leakage of the lubricant to sources of excitation, present in a typical drivetrain system.

According to the experimental findings of Silvestri et al. [21], radial vibration significantly affects the dynamic behaviour of lip seals, and at elevated excitation frequencies, the lip-seal material response is well represented by a non-linear Mooney–Rivlin formulation. The influence of viscoelastic material behaviour on the sealing performance of radial lip seals under dynamic excitation was also investigated by Xing et al. [22]. Their findings indicate that, at low rotational speeds, larger dynamic eccentricities may develop, which can lead to increased leakage. However, as the rotational speed rises and the shaft whirl approaches the dynamic eccentricity amplitude, the sealing performance tends to improve. They concluded that higher rotational speeds combined with increasing eccentric-

ity can elevate the likelihood of gap formation at the contact interface and the subsequent onset of leakage. The viscoelastic material behaviour of the radial lip can also impact its ability to follow the shaft displacement; hence, the gap in the contact is created as a result. More recently, Schollmayer et al. [23] investigated the followability of radial lip seals under dynamic shaft displacement. In their study, the shaft remained stationary (i.e., non-rotating), as the focus was solely on understanding the seal's ability to track lateral or radial shaft movements under dynamic excitation. Their results showed that, within excitation frequencies of approximately 0.1–1 Hz and displacement amplitudes between 10 and 200 µm, radial lip seals can lose their ability to follow such shaft motions across a relatively wide range of temperatures. They recommend extending the investigation to include cases where the shaft is also rotating, while simultaneously covering a broader range of operating temperatures.

It should also be noted that the vibration monitoring can aid with assessing the quality of the sealing performance. Zou et al. [24] investigated the vibration induced by the rotary shaft seal condition on the centrifugal pump performance experimentally. It was shown that vibration and the seal condition are interrelated phenomena. Seal-related mechanical behaviour has measurable vibration signatures, implying that dynamic excitation influences the interaction between the seal and shaft.

While several contributions have explored the effect of vibration or viscoelastic material behaviour, none have examined the combined influence of externally induced vibration and shaft surface topography on seal leakage. To determine the influence of vibration on the sealing performance, it is important to determine the vibration spectral characteristics of the system, frequency and amplitude. As the review of the literature and assessment of the prior research indicate, the important potential effects of propulsion system-induced vibrations on the driveline, including their influence on the transmission sealing system, have not hitherto been specifically investigated. This constitutes the knowledge gap and a motivation for the current research. This paper aims to specifically address this shortcoming by experimentally investigating the impact of externally induced vibrations on the sealing performance of radial lip seals. In particular, the role of the shaft surface topographical characteristics in the leakage performance under excitation conditions has also been investigated.

2. Front Wheel Drivetrain System

The driveshaft in a vehicle transmits the torque from the gearbox to the driven wheels. Figure 2 shows the driveshaft configuration for the front-wheel drive (FWD) vehicles. The driveshaft is an asymmetrically designed assembly of the gearbox (1). The driveshaft pieces represent the flexible parts of the driveline. They ensure the transmission of torque, regardless of the wheels' positions and orientation. The vehicle wheels must be able to steer freely at any time with no loss of drive power.

Due to the asymmetrical configuration, the driveshaft sections have different lengths. The right-hand-side Section (2) is elongated via a connecting shaft (3) to compensate for the eccentric position of the gearbox unit. The connecting shaft is supported by an additional bearing unit (4). For the driveshaft (5) on the left-hand side, no connecting shaft is required. Driveshafts can be structured into three components, comprising an inboard joint (6), a stub shaft (7), and an outboard joint (8) (Figure 2).

The outboard joint is a fixed joint. In addition to affecting steering kinematics, the outboard joint must compensate for deflection angle changes of up to 52°. All axial displacements are constrained. The outboard joint is connected to the wheels via a wheel hub. The inner joint must compensate for any deflections and rebound movements during driving. As the shock absorber deflects and retracts dynamically, the distance between the

wheels and the centre of the gearbox changes, owing to the tilting of the driveshaft. The maximum deflection angle for inboard joints is usually set to 28°. The inboard joint is also called a shift joint, because contrary to the restricted outboard joint, it can compensate for any axial movements.

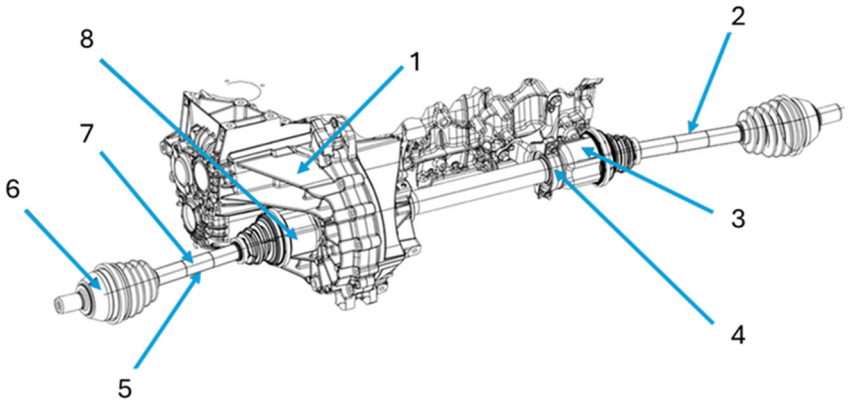

No.	Description
1	Gear Housing
2	Drive Shaft RHS
3	Linkshaft
4	Linkshaft Bracket
5	Drive Shaft LHS
6	Inboard Joint
7	IC-Shaft
8	Outboard Joint

Figure 2. Front-wheel drive configuration.

In the current study, tests were carried out both at a vehicle level and by using a representative test rig. The sealing system in the test rig is designed to be identical to that in the original transmission of the tested vehicle. Both the vehicle and the test rig are equipped with the same radial shaft seal. The radial lip seal consists of two sealing lips. The inner sealing lip is used to seal the lubricant from the air. The outer sealing lip serves as a barrier against the ingression of any contaminates into the sealing system. This can occur because of swirling dust and dirt during driving. In the assembled configuration, the sealing lip has a nominal contact width of 0.1–0.2 mm. The contact angle, α, on the front side of the seal is approximately 45°, whilst at the rear side, β is approximately 20° (Figure 3). The sealing lip is suspended elastically via a membrane, which allows the mating contacting surfaces to overlap. This leads an applied pressure on the mating interface. The pressure is increased by a tension spring.

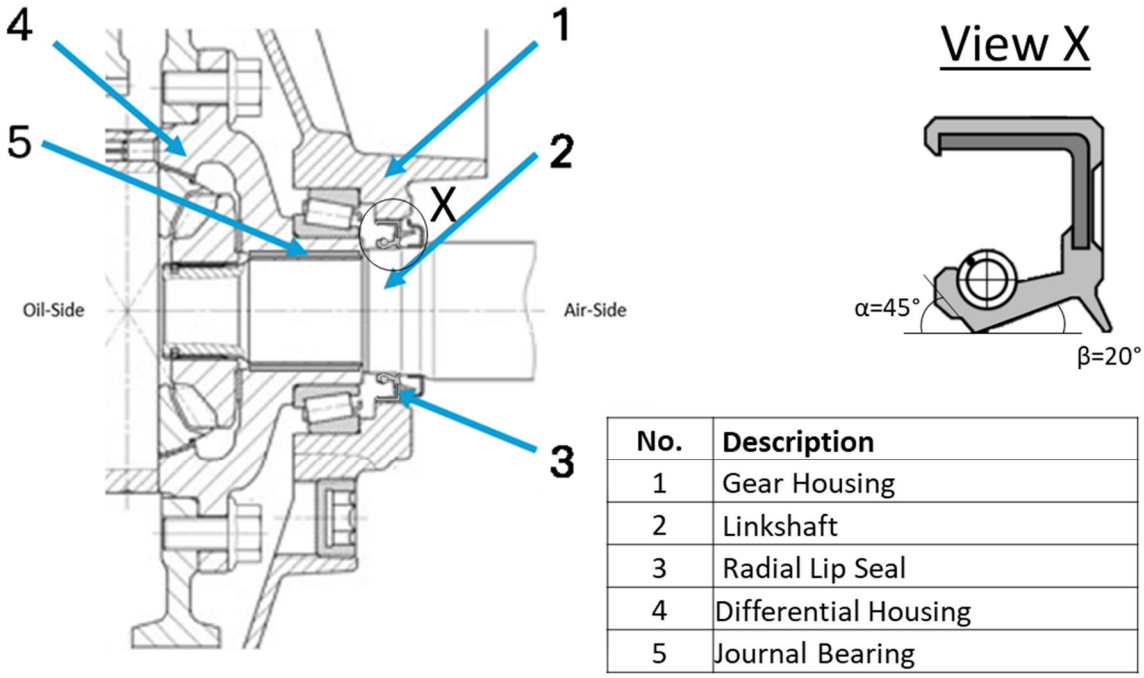

No.	Description
1	Gear Housing
2	Linkshaft
3	Radial Lip Seal
4	Differential Housing
5	Journal Bearing

Figure 3. The sealing system of the test vehicle transmission.

The sealing point between the differential and linkshaft of the test vehicle is shown in Figure 3. It comprises the gear housing (1), linkshaft (2), radial lip seal (3), differential housing (4) and the journal bearing support (5). The linkshaft (2) is connected to a side gear (2) through a mating spline. The shaft–seal conjunction consists of a radial lip seal (3) and a ground sealing seat at the linkshaft (2). The differential housing (4) is supported by a roller bearing within the gear housing (1). The linkshaft (2) is guided by a journal bearing (5), mounted onto the gear housing (1). The radial lip seal (3) comprises an inner elastomeric component, a stiffening ring and a tension spring. As the outer stiffening ring is pressed onto the bore of the gearbox housing, it statically pushes the lip seal against the gear housing (1).

2.1. Vehicle Test Procedure

The focus of this research is to enhance the understanding of the importance of vibrations on the sealing performance of transmission shafts, paired with radial lip seals. It is important to acquire measurements directly from a vehicle under real-world driving conditions. A test vehicle was fitted with miniature tri-axial accelerometers and comprehensive road tests were carried out. An overview of the accelerometers' attachment locations on the test vehicle drivetrain to measure system vibration is shown in Figure 4. A contactless rotary encoder (1) was used to measure the rotational speed of the toothed belt pulley mounted onto the crankshaft. A tri-axial accelerometer (2) was glued to the linkshaft bracket. A second accelerometer (3) was placed near the sealing interface of the linkshaft and the differential gear. Vibrations were measured by these accelerometers with the key objective of determining the onset of resonant behaviour in the vicinity of the driveshaft–gearbox seal. The resonant conditions may lead to increased amplitudes of oscillation and increased corresponding gaps in the sealing arrangement, thus potentially yielding rising levels of oil leakage, an aspect which is investigated in this study.

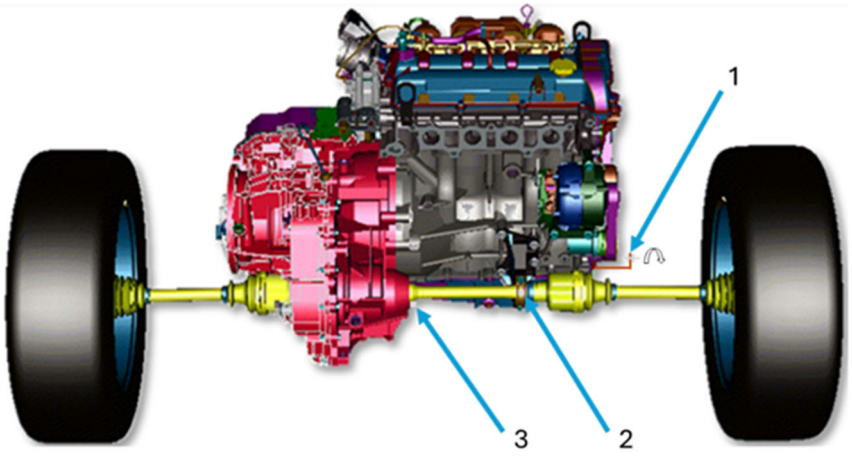

No.	Description
1	Rotary Encoder for Engine RPM
2	3D-Accelerometer Linksshaft-Bracket
3	3D-Accelerometer Differential-Interface

Figure 4. Positions for vibration sensing from FWD vehicle drivetrain system.

Figure 5a shows a non-contact inductive rotational encoder (6), employed to measure the engine rotational speed during the vehicle tests. For this study, the engine rotational

speed at which the tests were carried out was 800–1500 rpm during the various test drives. Measurements of engine speed were taken at 10 ms intervals.

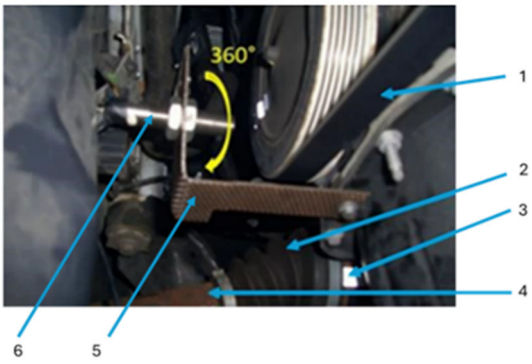

No.	Description
1	Tooth Belt
2	Bumper & Clamps
3	Inboard Joint
4	Drive Shaft (LHS)
5	Encoder Bracket
6	Rotary Encoder for Engine RPM

(**a**)

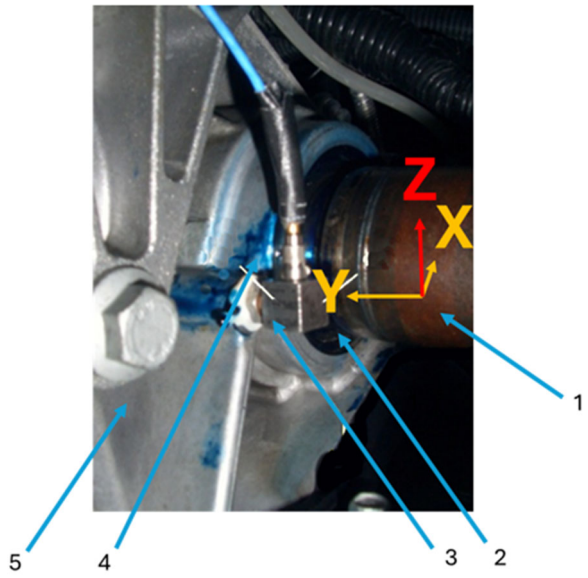

No.	Description
1	Linkshaft
2	Radial Lip Seal
3	3D-Accelerometer
4	Indicator Ink
5	Transmission Case

(**b**)

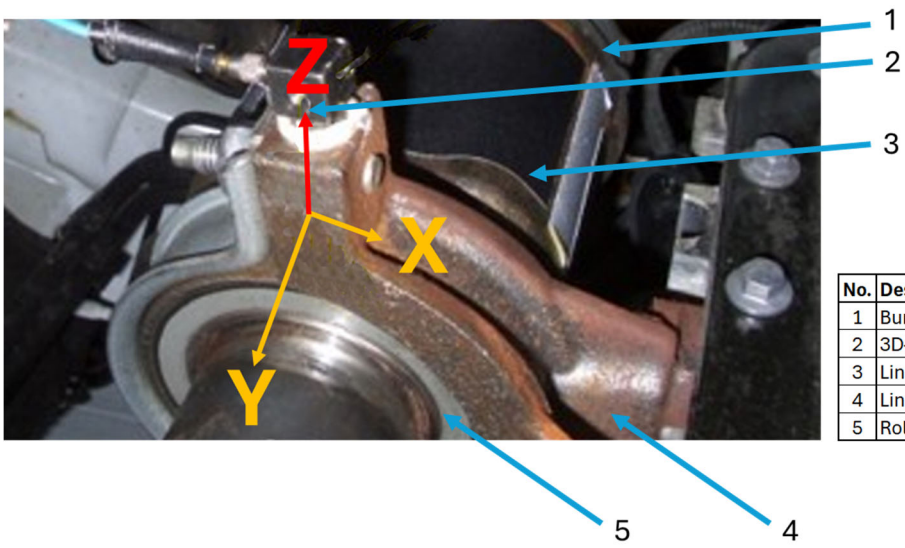

No.	Description
1	Bumper & Clamps
2	3D-Accelerometer - Linkshaft Bracket
3	Linkshaft
4	Linkshaft Bracket
5	Roller Bearing

(**c**)

Figure 5. (**a**) Rotary encoder for engine RPM, the triaxial accelerometer at the (**b**) differential-linkshaft interface, and (**c**) linkshaft bracket.

Figure 5b shows a tri-axial accelerometer (3) attached to the vehicle's transmission casing (5), monitoring vibrations. The surrounding area of the sealing system is formed by a linkshaft (1), a radial lip seal (2) and the transmission casing (5), marked with an indicator ink (4). The marking serves as a contrast medium for the improved visualisation of the

escaping transmission fluid when leakage occurs. This measuring area is of particular interest, as any leakage of oil escaping at this point may enter the environment as an ecologically hazardous substance. Figure 5c shows another tri-axial accelerometer (2) attached to the vehicle's linkshaft bracket (4). At this location, the vehicular drivetrain comprises the bumper with clamps (1), the linkshaft (3), the linkshaft bracket (4) and the roller bearing support (5). This measurement point is also of importance, as the potential excitation frequencies may be transferred to the sealing gap through the linkshaft.

The system's response to transient excitations from the drivetrain, as well as the road input, are measured by precision triaxial accelerometers of type PCB-HT356B21 (PCB Piezotronics, Inc., Depew, NY, USA), affixed by adhesives to the transmission cap at the interface with the linkshaft, as well as at the linkshaft support bracket, as shown in Figure 5b,c. These accelerometers have an operational integrity within the temperature range of −54 °C to +163 °C. Their measurement range is ± 4.909 m/s^2, with a sensitivity (resolution) of 0.04 m/s^2, and a frequency range of 2–10,000 Hz in the lateral Y and vertical Z-directions and 2–7000 Hz in the longitudinal X-direction (Figure 5b,c). The resonant frequency of the accelerometers is $\geq$55 kHz. The mass of the monitoring devices attached to the drivetrain components can potentially affect the system's spectral response. However, with a typical mass of 4 g, the accelerometers' influence on the response of the system is regarded as negligible.

The spectral response characteristics of the linkshaft bracket in the Z-Direction, during vehicle tests, show the Frequency Response Function (FRF) vibrational characteristics of the linkshaft bracket's vertical acceleration signal (Figure 6). The amplitude–frequency plot shows several peaks corresponding to the natural modal responses of the linkshaft bracket, noted by the instantaneous phase reversal of around 180 degrees in the frequency-phase response. These indicate modal responses at approximately 600 Hz, 1450 Hz and 2130 Hz in the monitored frequency range of 0–3000 Hz. High energy transfer occurs around these natural structural modes, with higher modal frequencies containing higher energy content. The significance of higher modal frequencies is in their elasto-acoustic nature, which is important for noise, vibration and harshness (NVH) analysis, but not so in the study of seal leakage. Therefore, if NVH refinement was the focus of the investigation, then higher modal responses of the bracket would be of primary interest. High modal responses give rise to the acoustic responses of drivetrain components: for example, in the driveline clonk phenomenon [25,26]. The real and imaginary components of the frequency response are shown in Figure 6a. The real component of the FRF represents the in-phase system response dominated by structural stiffness characteristics (flexible modal dynamics), whilst the imaginary contribution (response in quadrature) indicates the dominance of the inertial dynamics. Intersections of these response characteristics, shown in Figure 6b, represent rapid phase changes and the natural frequency peaks. Therefore, the interactions between structural and inertial dynamics, thus NVH performance and system compliance and ultimately seal leakage, can be thoroughly determined.

It is essential to measure the lubricant leakage from the lip seal simultaneously with the measurements of vibration, as described above. However, this is not possible in situ in vehicle tests, due to the significant complexities involved. By way of observation, vehicle tests have shown that vibration at natural modal responses of the vehicle linkshaft assembly leads to rising lubricant leakage, owing to increased oscillations at the transmission seal [27]. Consequently, a representative test rig needs to be developed and subjected to representative modal behaviour, although the rig modal characteristics would be marginally different to the vehicle, owing to the differences in the structural assembly. Nomikos et al. [28,29] described a test rig for measurement of leakage from the radial lip seal of a vehicular transmission casing. The study linked the surface topographical measures with

the leakage rate of the lubricant from the transmission seal. The same test rig is modified in the current study to relate the drivetrain vibrations (measured during vehicle tests) with the lubricant leakage, which can be measured accurately from the test rig. The test rig uses donor components from the test vehicle, such as the transmission, the linkshaft and the sealing system. Aspects of the test rig that are pertinent to the current study are detailed here.

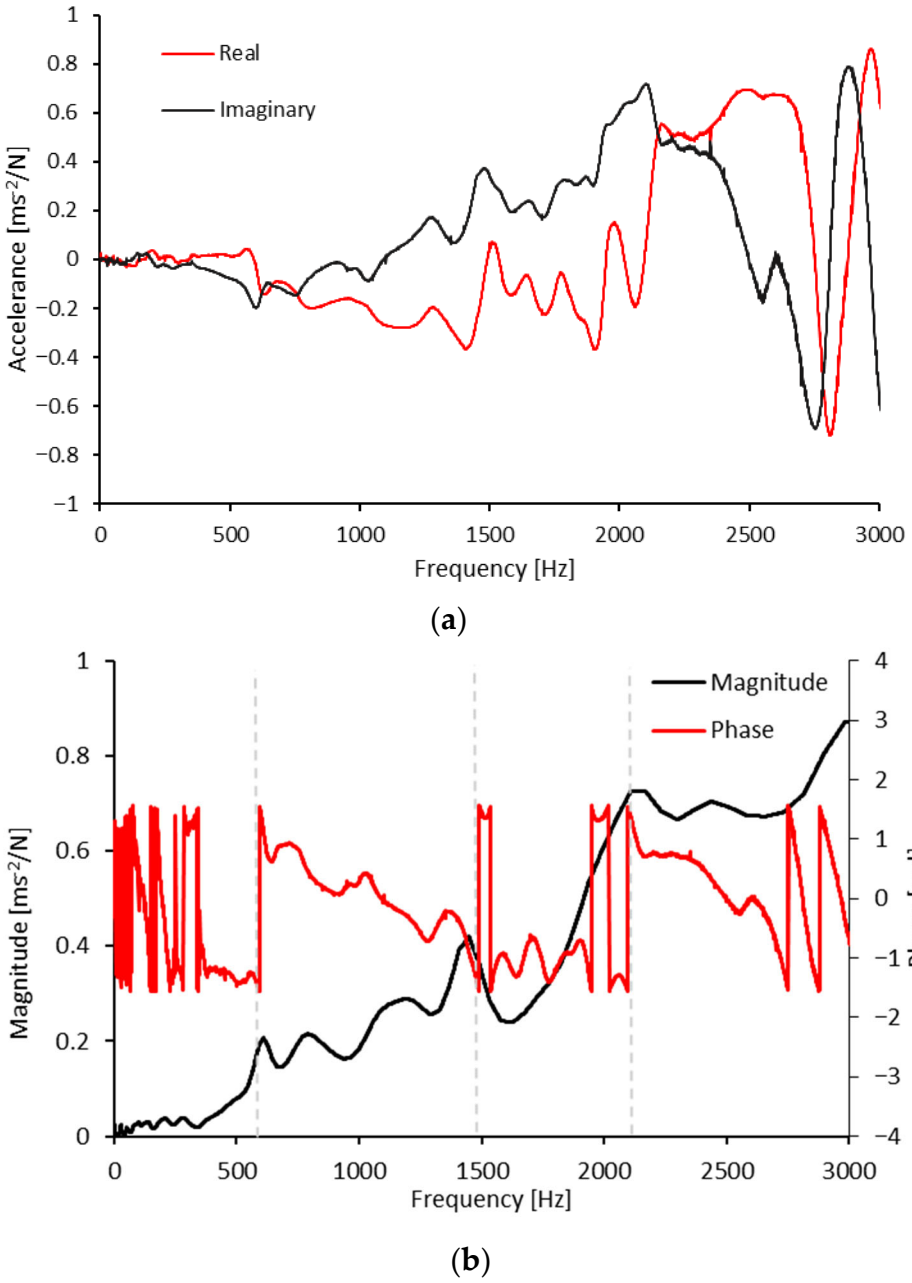

Figure 6. Spectral response characteristics of the linkshaft bracket in vehicle tests (**a**) real and imaginary parts and (**b**) the magnitude of acceleration and phase.

2.2. Drivetrain Test Rig

For the direct measurement of seal leakage and to ensure a repeatable testing procedure, it is essential to develop a specialised test rig that is representative of vehicle drivetrain operation in a controlled environment. The details of the developed testing are provided in [28]. The environment should facilitate the integration of multiple sensors and data acquisition systems. An important aim is to create a test environment closely

representing the real-world vehicle conditions, replicating the driveshaft assembly. The overall structure of the half-shaft assembly in the drivetrain system is shown in Figure 7. This includes the linkshaft assembly (1), the inter-connecting shaft (2) and the inboard-joint (3). The inner part of the inboard-joint assembly consists of a boot with clamps (3), roller (4), spider (5), needle bearing (6), grease (7), and the inboard joint (8).

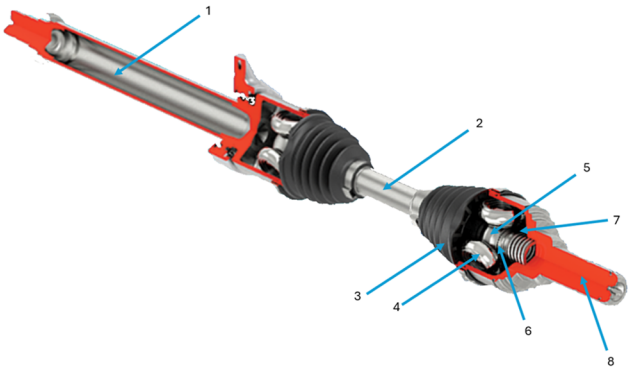

No.	Description
1	Linkshaft-Assembly
2	Inter-Connecting-Shaft
3	Boot with Clamps
4	Roller
5	Spider
6	Needle-Bearing
7	Grease
8	Inboard Joint (LHS)

Figure 7. Half-shaft assembly.

The primary components of the test rig, comprising the half-shaft assembly, are shown in Figure 8. The rig is mounted onto an adjustable heavy T-slot bed plate, making a test bench. All the test rig components are either from the donor vehicle itself or replicate the vehicle's exact specification. All the sensors used are the same as those employed in the vehicle tests. The shaker (vibration exciter) (1) used for system excitation in the Z-direction is mounted directly onto the linkshaft bracket (5), equipped with a tri-axial accelerometer (3). The linkshaft (4), as the test specimen, is assembled within the roller bearing of the linkshaft bracket (5). The inter-connecting (IC) shaft (2) is mounted onto the tripod of the linkshaft and connected to the drive motor of the test-rig. A second accelerometer (6) is employed for the modal analysis of the test stand to determine the natural frequency of the linkshaft assembly (4). A contactless rotary encoder (7) measures the shaft speed during the leakage tests. The rotary shaft seal (8) is mounted onto the sealing flange (9), which is fastened to the bearing flange (10), including a journal bearing. The linkshaft assembly (4) is supported on both ends; on the drive side by the linkshaft bracket (5) and on the gearbox side within the bearing flange (10). Additionally, accelerations of the gearbox are measured using a third accelerometer (11).

The sealing system at the core of the test rig is shown in Figure 9. It features a sealing area, designed to closely emulate that in the real test vehicle. For the test set-up, the donor vehicle parts are used. The original vehicle's journal bearing (5) is mounted onto the bearing flange (7). The linkshaft (2) is supported by a plain bearing seat. The sealing system comprises the radial lip seal (3) and the sealing seat of the linkshaft (2). It seals the oil side from the air side. The quantities of transmission oil leakage, which occur at the interface with the linkshaft, can be collected via a carefully placed blotting paper. Through weighing the paper prior to and post-test cycle, the weight difference yields the quantity of leaked oil. Two static sealing rings, placed between the differential housing (4) and the gear housing (1) prevent the leakage from the tank of oil. The bearing flange (6) and the sealing flange (7) are designed to be easily and flexibly interchangeable, thus enabling the test bench to be adapted for use with a wide range of vehicle types.

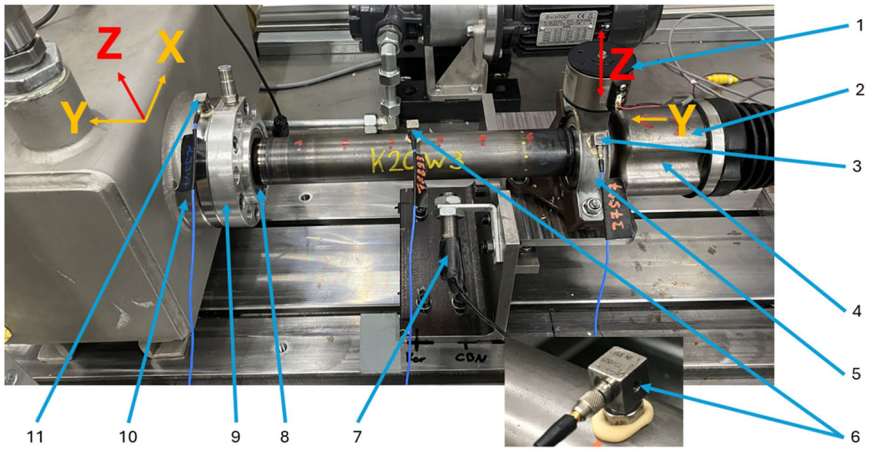

No.	Description
1	Shaker
2	IC-Shaft
3	3D-Accelerometer - Linkshaft Bracket
4	Linkshaft
5	Linkshaft Bracket
6	3D-Accelerometer - Linkshaft (Modal Analysis)
7	Rotarty Encoder for Engine RPM
8	Radial Lip Seal
9	Sealing-Flange
10	Bearing-Flange
11	3D-Accelerometer - Differential Interface

Figure 8. Dynamic drivetrain sealing test-rig.

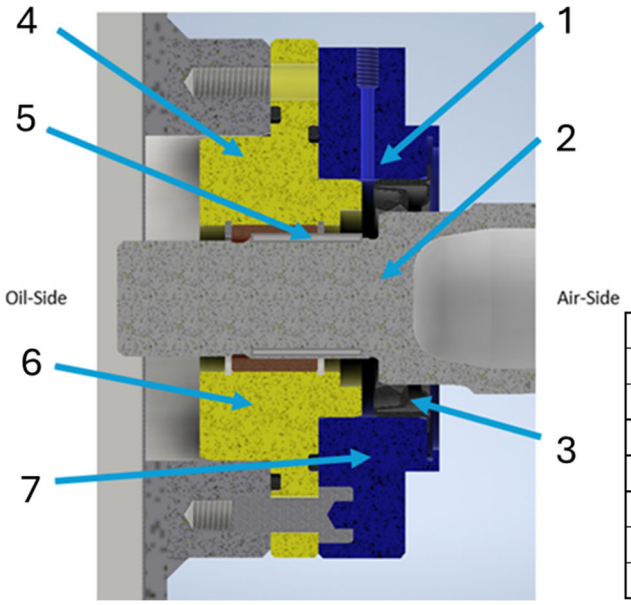

No.	Description
1	Gear Housing
2	Linkshaft
3	Radial Lip Seal
4	Differential Housing
5	Journal Bearing
6	Bearing-Flange
7	Sealing-Flange

Figure 9. Sealing system of the dynamic drivetrain sealing test-rig.

3. Experimental Results and Discussion

To ascertain the effect of vibration upon lubricant leakage, particularly with excitation at natural frequencies of the system, modal analysis should be carried out. As already stated, the natural frequencies of the test rig somewhat differ from that of the test vehicle, owing to the assembly constraints, which are naturally different. Therefore, experimental modal analysis based on impact hammer testing is carried out and system responses were measured at various locations, as indicated in Figure 10. Aside from the emergence of gaps in the sealing zone due to vibration, leakage is due to the surface topography in the contact,

as well as the driveshaft lead. Therefore, the experimental procedure should include the measurement of the shaft surface topography, as well as the shaft macro-lead geometry.

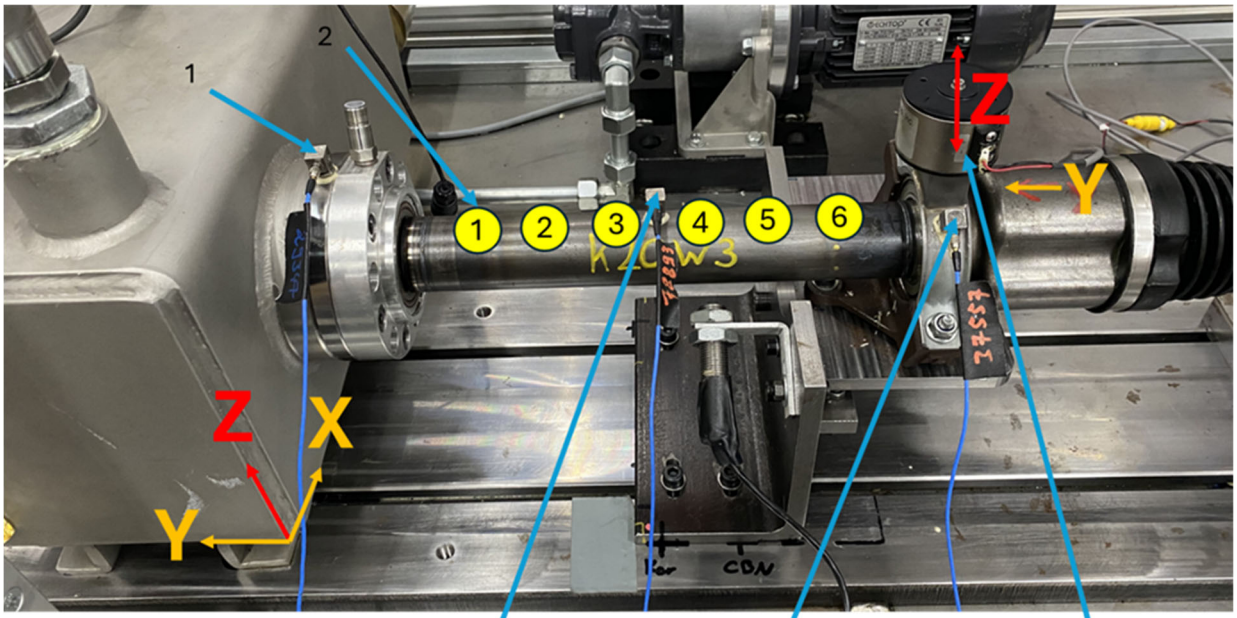

No.	Description
1	Measuring Point Differential
2	Impact Points 1–6
3	Measuring Point Linkshaft
4	Measuring Point Linkshaft-Bracket
5	Shaker

Figure 10. Structural modal determination.

3.1. Experimental Modal Analysis

The position of the vibration exciter (5) used to excite the test bench assembly in the vertical Z-direction is shown in Figure 10. A HEAD Recorder system was used for data acquisition during experimental modal analysis. An auto range process was executed, where repetitive impacts are made at a specific point on the object under investigation within an 8 s recurring time window. The measurements obtained during these strikes automatically adjust the processing software's parameters. The transient excitation signal is introduced into the system along the shaft at a theoretical distance of 35.375 mm, between the respective strike points in the Z-direction (Figure 10). This distance is derived from the total length of the shaft, which is 283 mm, with six defined impact points, with an accelerometer placed in the middle of the shaft. For each strike point, five excitation signals were generated, and their mean value was used for evaluation purposes. In addition, the vibrational behaviour was recorded at the simulated gearbox support locations on the left and at the OEM bracket on the right. The ArtemiS SUITE software, version 10.7, was used for the evaluation of the transfer functions.

The locations of the tri-axial accelerometers (1), (3) and (4) at measuring point (2) along the driveshaft specimen, as well as the linkshaft bracket, are shown in Figure 10. An impact hammer, model PCB 086C03, with a medium-hard plastic tip and a quartz-based load cell was used for modal testing. The hammer has a measuring range of ±2224 N with a sensitivity of 2.25 mV/N. The resonant frequency of the hammer itself is greater than 22 kHz, thus guarding against any interference in the measured readings of the structural responses of the test rig.

The spectrum of vibration of the linkshaft bracket in the vertical Z-direction is shown in Figure 11. The same observations can be made as those shown in Figure 6 for the

spectral characteristics of the linkshaft bracket in situ in the vehicle tests. The natural frequencies differ, as the assembly constraints for the linkshaft bracket within the test rig and in the vehicle drivetrain are not identical. The results show two natural frequencies in the range of 0–3000 Hz. These occur when there is a sharp reversal of around 180 degrees in the spectral phase, and occur at 967 Hz and 1490 Hz, respectively. Nevertheless, these natural frequencies are quite close to those measured in the vehicle tests. Clearly, the lower level of excitation energy generated by the impact hammer test compared with road input conditions means that the higher modal response at 2180 Hz obtained in vehicle tests is absent in the case of the test rig. Thus, the shaker can excite the test rig assembly at the measured natural frequencies of the linkshaft bracket, and the system response can be measured at the sites of the attached accelerometers.

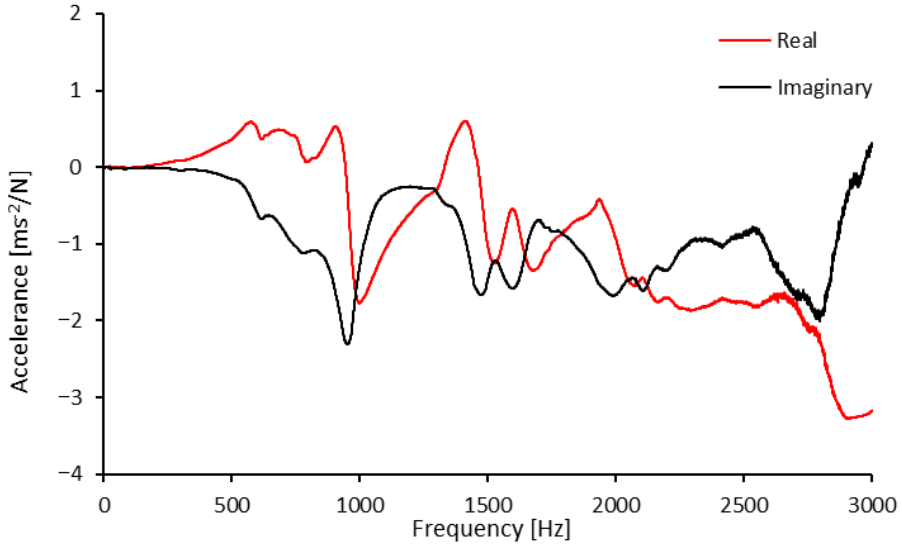

(**a**)

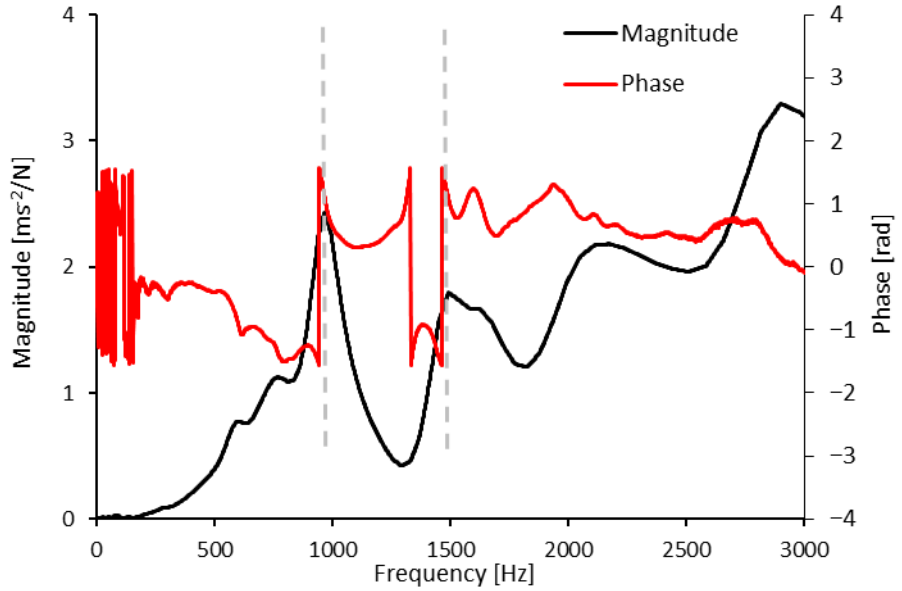

(**b**)

Figure 11. Spectral response of the linkshaft bracket in the test-rig (**a**) real and imaginary part and (**b**) magnitude of acceleration and phase.

3.2. Measurement of Surface Topography and Shaft Macro-Lead

The experimental investigation comprises the use of 10 driveshafts with ground sealing surfaces, using an abrasive grinding technique known as corundum grinding. Before use in the tests, surface roughness parameters Ra, Rz, and Ssk were measured for all the driveshafts' sealing surfaces, using a Keyence VK-9710 confocal 3D laser scanning microscope (Keyence Corporation, Osaka, Japan) with the magnification of 150×. The measurement field view was 70.61 µm × 93.66 µm. A helical structural profile is created during the machining of the driveshafts. This structure is referred to as a macro-lead, which induces lubricant conveyance flow along the shaft, which can promote leakage from the transmission seal. The shaft's macro-lead or helical structure was measured using a lead testing device: Hommel Etamic Formline F900 (Hommel Etamic–Jenoptik Industrial Metrology GmbH, Jena, Germany).

A typical microscopic image is shown in Figure 12. Ten individual measurements were undertaken for each driveshaft, and an average value was obtained in each case.

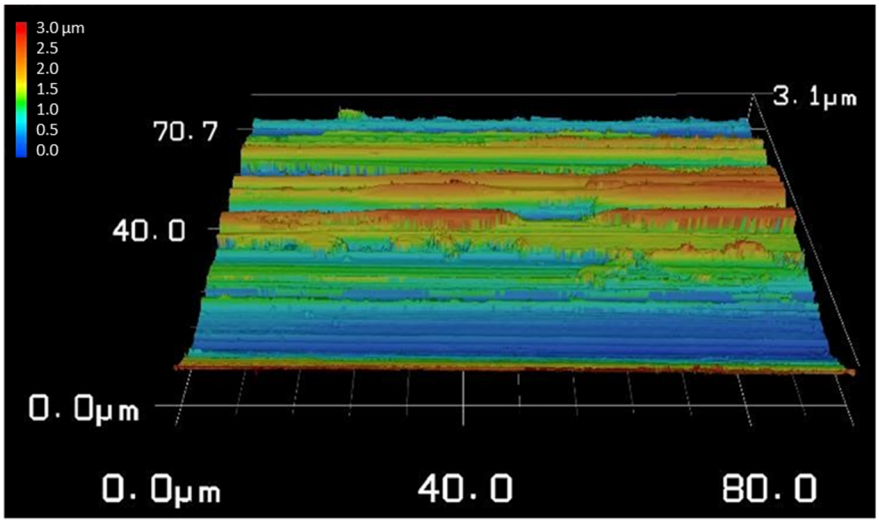

Figure 12. A typical microscopic image of the surface.

Table 1 lists the surface roughness measurements of the corundum ground driveshafts before and after a test cycle. One of the key surface roughness parameters listed is Rz. A decrease in the value of Rz prior to and after a test cycle suggests wear of the surfaces. For example, the driveshaft K20W01 shows a reduction in the Rz value from 3.526 µm to 2.021 µm, indicating wear (smoothening) of the rough surface topography.

The skewness, Ssk, of a surface is a measure of its topographical roughness heights' symmetry. A positive value indicates the dominance of asperity peaks in the surface topography, whilst a negative value signifies the predominance of valleys. The majority of Ssk values have reduced after completing a test cycle, suggesting an increased dominance of roughness valleys in the profile due to reduced asperity peak heights due to wear. Thus, a change in Ssk post-testing, such as in K20W01 from −0.112 to −0.205, implies a further transition towards valley-dominated surface topography, which is a characteristic of wear patterns in abrasive environments [30].

The average values of Rz, Ra and Ssk for the shafts presented in Table 1 are shown in Figure 13. The average Rz and Ra values have reduced after the tests, as shown in Figure 13, indicating the occurrence of shaft topography smoothening during the tests. The reduction in the Rz values suggests a reduction in peak heights. After the tests, the standard deviation in Ra values has also reduced (Figure 13), indicating a tendency towards a more uniform topographic profile, along with a reduction in the average Ra values. Figure 13 shows that

on average, the shafts' topographic skewness, excluding the two positive values, displays a reduction in peakiness, resulting in a roughness distribution with more significant valleys in the shafts' surfaces after tests.

Table 1. Measured surface topography.

Shaft	Rz [µm] Before Test	Rz [µm] After Test	Ra [µm] Before Test	Ra [µm] After Test	Ssk Before Test	Ssk After Test
K20W01	3.526	2.021	0.299	0.139	−0.112	−0.205
K20W02	2.831	1.623	0.185	0.086	−0.144	−0.264
K20W03	3.426	1.964	0.243	0.113	−0.141	−0.258
K20W04	4.108	2.355	0.265	0.123	−0.137	−0.252
K20W05	3.526	2.021	0.282	0.131	−0.029	0.054
K20W06	4.384	2.513	0.280	0.130	−0.264	−0.484
K20W07	4.249	2.436	0.825	0.383	−0.191	−0.351
K20W08	4.262	2.443	0.258	0.120	−0.272	−0.498
K20W09	4.176	2.394	0.413	0.192	−0.361	−0.662
K20W10	4.710	2.700	0.323	0.150	0.272	0.499

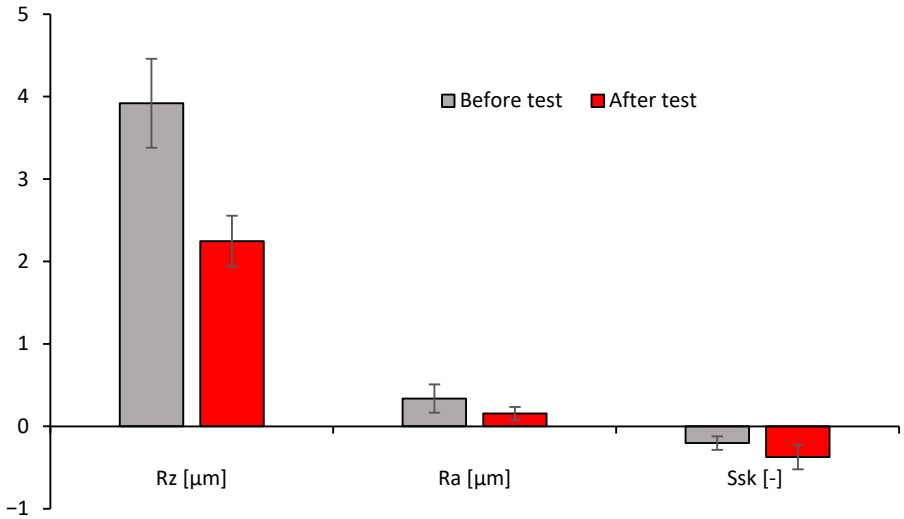

Figure 13. Average Rz, Ra, and Ssk values (excluding the two positive values) for the shaft surfaces measured before and after tests.

3.3. Measurement of Lubricant Leakage

The details of the lubricant leakage measurement have already been described in [28]. However, for the sake of completeness, a summary of the method is provided here. Leakage was measured using a direct approach, in which lubricant absorbed by a blotting paper, positioned at the seal outlet, was weighed using high-resolution laboratory scales. This method provides unambiguous and repeatable measurements of leaked mass and avoids uncertainties associated with indirect methods. Although commercial image-based leakage-detection systems exist, such a proprietary measuring system was not readily available for the purpose of the current study. Since the objective of this study is to correlate leakage behaviour with surface topographical parameters, a direct measurement of leaked mass is deemed to offer the most reliable basis for measurement. All tests were performed using Titan Sintofluid FE SAE 75W transmission fluid. To measure potential oil leakage, pre-cut and marked blotting papers were accurately weighed prior to testing. The paper

was positioned in a container and mounted under the sealing area. In this manner, the leaked lubricant could be collected throughout the test cycle. The blotting paper with the absorbed quantity of the leaked lubricant was weighed after the test cycle and compared with its pre-test weight, using a Toledo Mettler AT 250 precision scale (Mettler Toledo, Columbus, OH, USA). Based on the surface characteristics, the sealing performance of the shafts, while rotating at 1000 RPM, was tested by measuring leakage in grams per 20 h test duration under two different conditions: with and without imposed vibration in the Z-direction at the measured resonant frequency of 967 Hz for the test rig. A K2002E01 miniature electrodynamic inertial shaker (The Modal Shop, Inc., Cincinnati, OH, USA) was used, which is capable of providing an excitation frequency in the range of 20–3000 Hz, with maximum peak-to-valley displacement and peak velocity of 8.9 mm and 508 mm/s, respectively. The choice of test duration has been extensively discussed in [28]. Briefly, the leakage from the tested shafts during the break-in cycle was considered in all tests. During this phase, the variations in applied torque over time was recorded, with the aim of maintaining a constant rotational speed. The break-in point was considered to be the moment when the initial high measured torque falls to a minimum, after which the monitored torque remains largely settled and thereupon does not show any significant variations. It was observed that most leakage occurs during the initial break-in period, after which the leakage rate is significantly reduced. However, because the monitoring of surface roughness variations in time during the tests is not possible, all the shafts were exposed to a 20-hr period of the break-in process in order to ensure that all shaft surfaces have reached their break-in points.

The tests were conducted under ambient temperature conditions of around 25 °C, while the oil sump temperature was kept at 60 °C. This was achieved through a specifically designed control system for the operation and monitoring of the test rig, as described in detail [28,29]. Two heating elements were installed in the lubricant tank to enable precise adjustment and control of the sump temperature. Additionally, the temperature of ambient air was recorded and could be adjusted by an air conditioning unit. The control of the test-stand was ensured through a programmable digital control, operated by means of an HMI (human–machine interface). A sensor control unit was used on each sensor tip, which transmits the relevant detected signals to the I/O-link master.

Table 2 lists the measured leakage from the shaft–seal conjunction without any imposed excitation. The measurements correspond to the driveshafts with different macro-lead angles.

Table 2. Measured oil leakage without system excitation, using blotting paper mass variation.

Shaft	Lead Angle [°]	Mass Before Test [g]	Mass After Test [g]	Mass Difference [g]
K20W01	0.435	0.915	1.179	0.264
K20W02	0.410	0.950	1.003	0.053
K20W03	0.419	0.926	0.928	0.002
K20W04	0.440	0.944	1.149	0.205
K20W05	0.558	0.939	4.074	3.135
K20W06	0.460	0.913	1.387	0.474
K20W07	0.480	0.935	1.011	0.076
K20W08	0.470	0.934	1.444	0.510
K20W09	0.410	0.934	0.941	0.007
K20W10	0.536	0.945	2.604	1.659

The variation in the measured oil leakage with the lead angle is shown in Figure 14. Clearly, there is an indication of an exponential relationship between the oil leakage and the shaft lead angle (as the oil leakage rises significantly with relatively small changes in the shaft lead angle). This rise is an expected outcome, as larger lead angles cause greater lubricant flow through helical conveyance. However, the exact nature of the detailed relationship between the leakage and the lead angle requires further investigation, including further data, to clarify the observed trend.

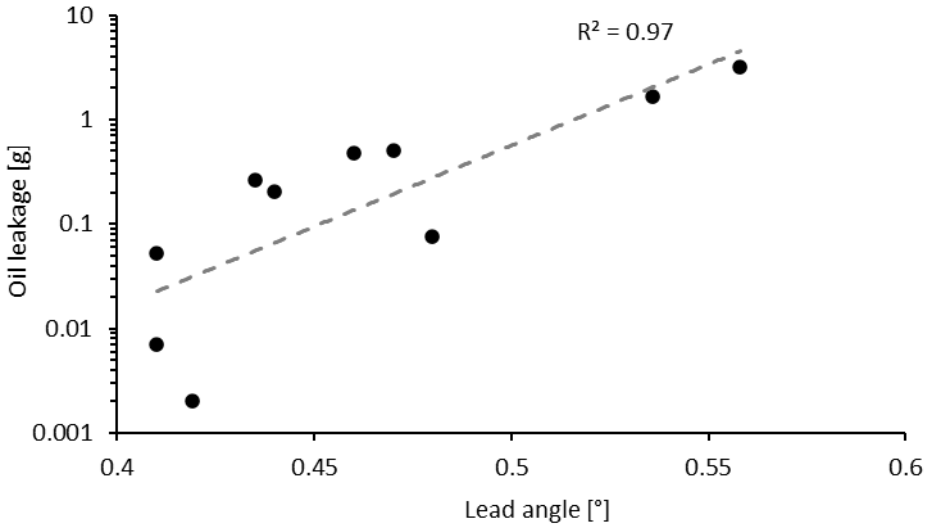

Figure 14. Variations in oil leakage with lead angle with no excitation (dots represent measured data points, and the dashed line shows the corresponding trend line).

The results with and without linkshaft bracket excitation at the natural frequency of 967 Hz are shown in Table 3. The table also includes the results of topographical measurements Rz, Ra, and Ssk for all shafts after the first test cycle.

Table 3. Measured oil leakage with and without system excitation.

Shaft	Rz [µm]	Ra [µm]	Ssk [-]	Leakage [g] Without Excitation	Leakage [g] with Excitation
K20W01	2.021	0.139	−0.205	0.264	4.124
K20W02	1.623	0.086	−0.264	0.053	3.698
K20W03	1.964	0.113	−0.258	0.002	3.753
K20W04	2.355	0.123	−0.252	0.205	4.245
K20W05	2.021	0.131	0.054	3.135	5.630
K20W06	2.513	0.130	−0.484	0.474	2.965
K20W07	2.436	0.383	−0.351	0.076	3.491
K20W08	2.443	0.120	−0.498	0.510	2.821
K20W09	2.394	0.192	−0.662	0.007	1.928
K20W10	2.700	0.150	0.499	1.659	6.184

For the corundum-ground shafts under investigation, the value of Rz ranges from 1.623 µm (K20W02) to 2.700 µm (K20W10). This is within the range specified by various standards for the shaft roughness (1.2–3.0 µm) [5,31,32]. The Ra value varies between 0.086 µm (K20W02) and 0.383 µm (K20W07), which are again in the range specified by the standards (0.2–0.5 µm) [5,31,32]. The skewness, Ssk, value provides an insight into the

surface topographical asymmetry, as already described, with negative values indicating valley-dominated topography.

The results for the measured oil leakage rate with and without the linkshaft bracket extradition are shown in Figure 15. The results indicate that seal leakage in the absence of imposed vibration is generally lower, with a minimum of 0.002 g/20h (K20W03) and a maximum of 3.135 g/20 h (K20W05). With excitation near resonant vibration at 967 Hz, lubricant leakage increases significantly, with the highest recorded value at 6.184 g/20 h (K20W10). This is in line with the observation of loss of seal followability under shaft oscillatory displacement, as reported in [23]. This is the case for all of the shafts. The data suggest that the surface characteristics of the shafts, particularly the skewness parameter, influence the leakage behaviour both with and without excitation. The trendlines in Figure 15 suggest that as the skewness increases, the leakage rate also rises, reaching levels of up to 6.184 g/20 h at the highest measured Ssk value with the presence of vibrations. This is quite significant. The trendline has a more gradual rise without vibration excitation rising to a leakage rate of 1.3 g/20 h. The leakage rate increases with Ssk, particularly in the presence of vibration.

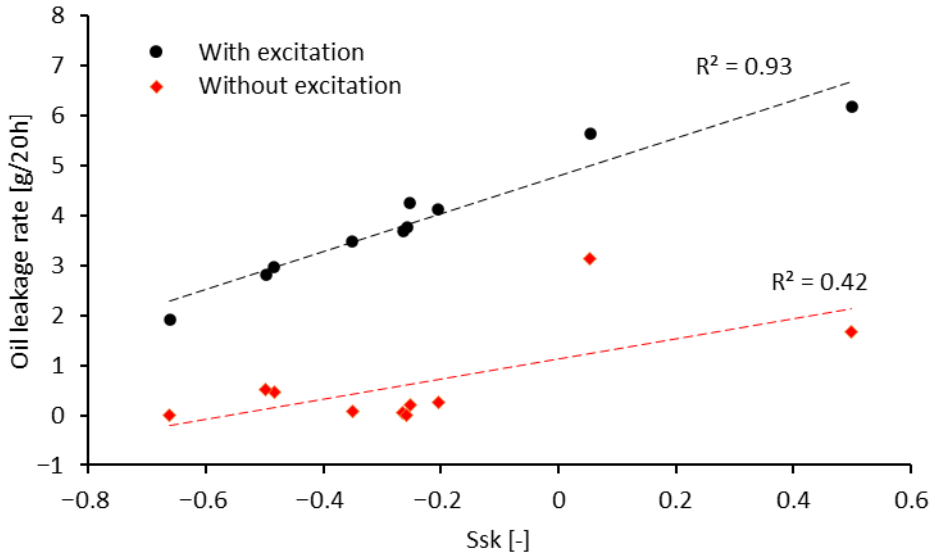

Figure 15. Variation in seal leakage rate with shaft surface skewness profile with and without the presence of vibrational input.

Statistical analysis of the data confirms a strong correlation between Ssk and leakage under excitation (Pearson r = 0.97, $p < 10^{-5}$; Spearman ρ = 0.99, $p < 10^{-7}$). Without excitation, the correlation seems to be moderate (r = 0.65, $p = 0.043$; ρ = 0.44, $p = 0.20$). This is consistent with the lower $R^2 = 0.42$ observed in Figure 15. Linear regression analysis also shows that the slope under non-excited conditions is still statistically significant at the 95% confidence level. A Fisher r-to-z comparison also demonstrates that the correlation is significantly stronger with excitation ($z = -2.35$, $p = 0.019$). This indicates that vibration markedly enhances the dependence of leakage on surface skewness.

Shafts with negative Ssk values, indicative of valley-dominated surfaces, generally show lower leakage rates, especially under vibration. Conversely, shafts with positive Ssk values, characterised by peak-dominated surfaces, tend to exhibit higher leakage, particularly under excitation at higher frequencies. A significantly better correlation between the leakage rate and shaft skewness values is also noted, indicating that the inclusion of any excess vibrations in the system can exacerbate leakage for shafts with less negative or positive skewness profiles, as the shaft surface profile deviates further from an optimum one. Similarly to the results shown by the authors [28], no specific correlations between

the measured leakage rate and the shaft roughness parameters such as Ra and Rz were observed, with the inclusion of system excitation, as the data shown in Table 3 indicate.

A positive skewness may enhance the fluid flow by providing pathways along asperity peaks, which become more pronounced with vibrations. Thus, surface profile asymmetry has a critical role in the leakage behaviour. This highlights the importance of controlling the surface profile asymmetry, particularly in applications where significant vibrations are present.

Since each shaft possesses its own unique surface topographical characteristics, if the same shaft is used for a multitude of tests, both the seal and the shaft roughness alter after each run. As the result, the leakage measured in any subsequent test would correspond to a shaft with the altered roughness properties. This means that effectively, each repeated test would represent a different data point in Figure 15. For this reason, the standard practice of repeating each test several times to obtain a mean and standard deviation was not applicable in the context of the current study. Furthermore, it is important to highlight that further numerical analysis and/or experimental tests are required to investigate the impact and contribution of parameters such as the local heating and its dissipation through various thermal pathways, due to generated frictional torque [29], as well as local seal degradation under long duration running conditions on the results.

4. Conclusions

A test rig has been designed and manufactured to emulate the in-vehicle shaft-seal contact resonant conditions, using actual components from a donor vehicle. The measurements of leakage presented in this paper underscore the critical role of the shaft surface roughness parameters in influencing the sealing performance at vehicular gearboxes. The analysis reveals that while all corundum-ground shafts exhibit some degree of leakage, significant variations occur under different excitation conditions.

The data indicates that the skewness parameter Ssk is particularly influential. Shafts with positive skewness show markedly higher leakage rates when subjected to vibration at a structural modal response of 967 Hz. Conversely, shafts characterised by negative Ssk values, indicative of valley-dominated surfaces, tend to maintain lower leakage rates, especially in the absence of vibration. The Rz and Ra parameters, while relevant, demonstrate a weaker correlation with leakage rates, suggesting that surface asymmetry plays a more decisive role in fluid dynamics under vibrational conditions.

These findings highlight the necessity of controlling surface profile asymmetry in applications subjected to vibration, as the geometry of the sealing interface significantly impacts the performance of shaft seals. The results presented here provide important insights for the design and optimisation of sealing solutions in automotive and potentially aerospace and wider engineering applications, emphasising the importance of careful consideration of surface characteristics to enhance leakage performance. Use of appropriate machining and grinding processes for the shaft to achieve the desired surface topography attributes is a key aspect that needs to be investigated and adapted carefully for any specific application requirements. Furthermore, the contamination of the contact in real-world application and its potential effect on the surface topography needs to be considered.

Significantly, this study underscores a need to update the existing standards (e.g., [4–6]) for shaft roughness and topographical characteristics when pairing them with radial lip seals. The existing standards specify the surface roughness parameters such as Ra and Rz for shafts. However, the extensive set of analysis carried out in this research, together with previously published work on the same research programme (e.g., [12,28]), clearly demonstrates that the existing standards need to be revised to incorporate more specific and relevant guidelines for shaft roughness specifications such as surface roughness skewness

and kurtosis when in contact with radial lip seals. Implementing this, however, may require further tests with various machined and ground shaft surface profiles and lip seal designs and geometries, and under different operations, in order to find a more robust recommended range for shaft roughness parameters that covers wider applications and conditions than those considered in this set of studies. Additional factors that may influence the measurements, such as local heating in the sealing contact, potential local seal material degradation during excitation, uncertainties associated with vibration transmission, and limitations in data acquisition, will also need to be considered in future extensions of this research.

Author Contributions: Conceptualization, P.N. and R.R.; methodology, P.N. and R.R.; software, P.N.; validation, P.N.; formal analysis, P.N. and R.R.; investigation, P.N.; resources, P.N.; data curation, P.N.; writing—original draft preparation, P.N.; writing—review and editing, P.N., N.M., H.R. and R.R.; visualization, P.N., N.M. and R.R.; supervision, N.M. and R.R.; project administration, P.N. and R.R.; funding acquisition, P.N. and R.R. All authors have read and agreed to the published version of the manuscript.

Funding: This project was funded by Neapco Europe.

Institutional Review Board Statement: Not applicable.

Informed Consent Statement: Not applicable.

Data Availability Statement: The raw data supporting the conclusions of this article will be made available by the authors on re-quest.

Acknowledgments: The authors would like to acknowledge the financial contributions of Neapco Europe towards work carried out in this project.

Conflicts of Interest: Author Petros Nomikos was employed by the company Neapco Europe GmbH. The remaining authors declare that the research was conducted in the absence of any commercial or financial relationships that could be construed as a potential conflict of interest.

Abbreviations

DIN	Deutsches Institut für Normung
FEA	Finite Element Analysis
FRF	Frequency Response Function
FWD	Front Wheel Drive
ISO	International Standard Organisation
NVH	Noise, Vibration and Harshness
OEM	Original Equipment Manufacturer
Ra	Arithmetic Mean Roughness
RMA	Rubber Manufacturing Association
Rq	Root Means Square Roughness
RWDR	Rotary Shaft Seal (Radialwellendichtring)
Rz	Peak to Valley Surface Roughness
Ssk	Skewness of Surface Roughness
TÜV	Technical Supervisory Association (Rhineland)

References

1. Simmer, W. Aus Elastischem Werkstoff Bestehende Dichtung Für Umlaufende Wellen Oder Hin Und Her Gehende Stangen. Patentschrift DE729128C, 27 February 1938.
2. TÜV SÜD. Die Häufigsten Mängel Beim Auto. 2021. Available online: https://www.tuvsud.com/de-de/publikationen/tuev-report/die-haeufigsten-maengel (accessed on 1 January 2025).

3. Jagger, E.T. Rotary shaft seals: The sealing mechanism of synthetic rubber seals running at atmospheric pressure. *Proc. Inst. Mech. Eng.* **1957**, *171*, 597–616. [CrossRef]
4. *DIN 3761-9:1984-01*; Rotary Shaft Seals for Motor Vehicles—Radial Force; Testing of Radial Force. DIN: Berlin, Germany, 1984; pp. 71–75.
5. RMA. *OS1-1 Oil Seal Technical Bulletin—Shaft Requirements for Rotary Lip Seals*; Rubber Manufacturers Association: Washington, DC, USA, 2004; pp. 2–10.
6. *DIN ISO 6194-1*; Rotary Shaft Lip-Type Seals Incorporating Elastomeric Sealing Elements—Part 1: Nominal Dimensions and Tolerances. DIN: Berlin, Germany, 2007; pp. 18–26.
7. Salant, R.F. Modelling rotary lip seals. *Wear* **1997**, *207*, 92–99. [CrossRef]
8. Upper, G. Dichtlippentemperatur von Radialwellendichtringen. Ph.D. Thesis, Karlsruhe University, Karlsruhe, Germany, 1968.
9. Kang, Y.S.; Sadeghi, F. Numerical analysis of temperature distribution at the lip seal–shaft interface. *J. Tribol.* **1997**, *119*, 273–278. [CrossRef]
10. Buhl, S. Wechselbeziehungen im Dichtsystem von Radial-Wellendichtring, Gegenlauffläche und Fluid. Doctoral Dissertation, Institute for Machine Elements, University of Stuttgart, Stuttgart, Germany, 2006. Report 117.
11. Salant, R.F.; Shen, D. Hydrodynamic effects of shaft surface finish on lip seal operation. *Tribol. Trans.* **2002**, *45*, 404–410. [CrossRef]
12. Kozuch, E.; Nomikos, P.; Rahmani, R.; Morris, N.; Rahnejat, H. Effect of shaft surface roughness on the performance of radial lip seals. *Lubricants* **2018**, *6*, 99. [CrossRef]
13. Amabili, M.; Colombo, G.; Prati, E. Experiments on the dynamics of a rubber ring seal. In Proceedings of the 17th International Modal Analysis Conference (IMAC), Orlando, FL, USA, 8–11 February 1999; pp. 297–301.
14. Silvestri, M.; Prati, E. Frictional Behaviour of Radial Lip Seals on Varying Exerted Pressure. In Proceedings of the 14th Nordic Symposium on Tribology, Lulea, Sweden, 8–11 June 2010.
15. Lee, F.; Wu, W.; Zhao, M.; Ghaffari, M.; Liao, L.; Siegel, D. Prognostics and health management design for rotary machinery systems—Reviews, methodology and applications. *Mech. Syst. Signal Process.* **2014**, *42*, 314–334. [CrossRef]
16. Talikoti, B.S.; Kurbet, S.N.; Kuppast, V.V. A review on vibration analysis of crankshaft of internal combustion engine. *Int. Res. J. Eng. Technol.* **2015**, *2*, 1943–1948.
17. Kumar, A.; Patil, P.P. Modal analysis of heavy vehicle truck transmission gearbox housing made from different materials. *J. Eng. Sci. Technol.* **2016**, *11*, 252–266.
18. Oehlmann, H.; Brie, D.; Tomczak, M.; Richard, A. A method for analysing gearbox faults using time–frequency representations. *Mech. Syst. Signal Process.* **1990**, *11*, 529–545. [CrossRef]
19. Tuma, J. Gearbox noise and vibration prediction and control. *Int. J. Acoust. Vib.* **2009**, *14*, 99–108. [CrossRef]
20. Lei, Y.; Han, D.; Lin, J.; He, Z. Planetary gearbox fault diagnosis using an adaptive stochastic resonance method. *Mech. Syst. Signal Process.* **2013**, *38*, 113–124. [CrossRef]
21. Silvestri, M.; Prati, E.; Tasora, A. Radial lip seals efficiency under dynamic operating conditions. In Proceedings of the International Conference on Tribology, Parma, Italy, 20–22 September 2006; Volume 5, pp. 20–22.
22. Xing, Y.; Zhai, F.; Li, S.; Wang, X.; He, Z. A study on radial oil seal leakage failure due to viscoelasticity under dynamic eccentricity. *Ind. Lubr. Tribol.* **2024**, *76*, 1197–1204. [CrossRef]
23. Schollmayer, T.; Thielen, S.; Schröder, V.; Sauer, B.; Koch, O. Experimental investigation of the radial shaft seal followability against dynamic shaft displacement without shaft rotation at low temperatures. *J. Tribol.* **2025**, *147*, 104401. [CrossRef]
24. Zou, J.; Luo, Y.; Han, Y.; Fan, Y.; Wang, C. Investigation on the vibration induced by the rotary-shaft-seal condition in a centrifugal pump. *Sensors* **2025**, *25*, 5399. [CrossRef] [PubMed]
25. Krenz, R. Vehicle response to throttle tip in/tip out. *SAE Tech. Pap.* **1985**, *94*, 850967.
26. Rahnejat, H.; Johns-Rahnejat, P.M.; Dolatabadi, N.; Rahmani, R. Multi-body dynamics in vehicle engineering. *Proc. Inst. Mech. Eng. Part K—J. Multi-Body Dyn.* **2024**, *238*, 3–25. [CrossRef]
27. Nomikos, P.; Kozuch, E.; Morris, N.; Rahmani, R.; Rahnejat, H. Measurement of vibrations affecting the power transmission seals. In Proceedings of the 4th Biennial International Conference on Powertrain Modelling and Control (PMC 2018), Loughborough, UK, 10–11 September 2018.
28. Nomikos, P.; Rahmani, R.; Morris, N.; Rahnejat, H. An investigation of oil leakage from automotive driveshaft radial lip seals. *Proc. Inst. Mech. Eng. Part D—J. Automob. Eng.* **2023**, *237*, 3108–3124. [CrossRef]
29. Nomikos, P.; Rahmani, R.; Morris, N.; Rahnejat, H. Measurement and prediction of thermal performance of automotive transmission radial lip seals. *Proc. Inst. Mech. Eng. Part D—J. Automob. Eng.* **2025**, *239*, 1367–1383. [CrossRef]
30. Duo, Y.; Tang, J.; Zhao, Z.; Shengyu, Y.; Li, G.; Zhu, G. Discrimination of wear performance based on surface roughness parameters arithmetic mean height (Sa) and skewness (Ssk). *Wear* **2024**, *548*, 205397. [CrossRef]

31. *ISO 4288:1996*; Geometrical Product Specifications (GPS)—Surface Texture: Profile Method—Rules and Procedures for the Assessment of Surface Texture. International Organization for Standardization: Geneva, Switzerland, 1996.
32. *DIN 4768:1990-05*; Determination of Values of Surface Roughness Parameters Ra, Rz, Rmax Using Electrical Contact (Stylus) Instruments—Concepts and Measuring Conditions. DIN: Berlin, Germany, 1990.